

Artifact analysis on triangular box-spline and subdivision meshes

U. H. Augsdörfer^a, N. A. Dodgson^a, M. A. Sabin^b

^a*Computer Laboratory, University of Cambridge, 15 J. J. Thomson Ave, Cambridge CB3 0FD, England*

^b*Numerical Geometry Ltd., 19 John Amner Close, Ely, Cambridge CB6 1DT, England*

Abstract

Artifacts are present in subdivision and box-spline surfaces (Sabin and Barthe, 2003; Sabin et al., 2005; Augsdörfer et al., 2009). An artifact is a feature of the limit surface which cannot be avoided by movement of control points by the designer. Ideally, the difference between designer intent and what emerges as a limit surface should be eliminated. The first step to achieving this is by understanding and quantifying the artifact observed in the limit surface.

Utilising the subdivision process as a tool for analysis we develop a generic expression to determine the magnitude of artifacts in the limit surface. Our results provide a measure of artifacts present in the limit surface with respect to initial control point sampling. We demonstrate the method by analysing box-splines and subdivision surfaces based on triangular meshes: Loop subdivision, Butterfly subdivision and a novel interpolating scheme with two smoothing stages.

Key words: subdivision, artifact, Loop subdivision, butterfly subdivision

1. Introduction

Subdivision is an algorithmic technique to generate smooth surfaces as the limit of a sequence of successively refined polygons or polyhedra. The limit surface is made up of components with spatial frequencies below the Nyquist limit and those with spatial frequencies above. The designer can control the first group of components by moving control points, and so this group gives in some sense the desired surfaces. However, the designer cannot control the second group and these are what we call artifacts.

To be able to make an appropriate choice of which scheme and how many control points to use, the designer needs to know how the artifacts vary with the scheme and sampling density. Sabin et al. (2005) explained how subdivision can be employed as a tool for analysis of artifacts which are not controllable by the designer. Augsdörfer et al. (2009) extended this idea to limit surfaces based on quadrilateral meshes. In this work we develop a generic expression based on the tools described by Sabin et al. (2005) which is applicable to limit surfaces irrespective of the mesh type. We demonstrate this method by analysing, for the first time, box-splines and subdivision surfaces based on triangular meshes. The three examples analysed are limit surfaces

Email addresses: Ursula.Augsdorfer@cl.cam.ac.uk (U. H. Augsdörfer), Neil.Dodgson@cl.cam.ac.uk (N. A. Dodgson), malcolm@geometry.demon.co.uk (M. A. Sabin)

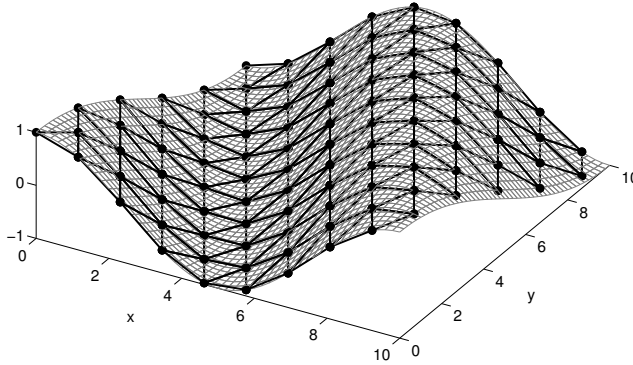


Figure 1: A triangular mesh (black) of the form $\cos(\pi\Omega \cdot 2J)$ sampled from a sinusoidal surface (grey). In this example $\Omega = [0.1, 0.2]$. Points indicate the vertices of the control polyhedron.

obtained using Loop subdivision (Loop, 1987), Butterfly subdivision (Dyn et al., 1990) and a novel interpolating subdivision scheme with two smoothing stages.

2. Method of Analysis

One subdivision step can be viewed as a multi-stage process involving one refinement stage followed by one or more smoothing stages. Sabin et al. (2005) showed that artifact components are inevitably introduced in the refinement stage. The signal and the artifact components are then both smoothed in subsequent smoothing stages. When handling schemes not based on box-splines we may encounter, next to refinement and smoothing stages, a kernel from which no more smoothing stages can be extracted. In these cases, we need to determine the kernel's effect. We also want to determine the magnitude of the artifact in the limit surface, and so the effect of the limit stencil, different for each scheme, must be considered.

2.1. The input surface

In order to analyse the behaviour we sample original data, A_J , from a 2D sine wave of frequency Ω , measured in units of complete cycles per original vertex. An actual data set can be regarded as the sum of such components by Fourier theory, and, because the system updating from one step to the next is linear, we can separate the initial data into components of different spatial frequency, and look at the response of each component as a function of frequency. The effect on the total is the sum of the effects on the separate spatial frequency components.

We use $J = (x, y)$ to denote the grid points before refinement and P for the grid points after refinement.

In triangular grids we have three principal grid directions X_1, X_2 and X_3 , each of which is given as a vector $X_k = [x_k \ y_k]$, where $k \in \{1, 2, 3\}$ (see Figure 2 for labelling). Each sample point A_J on the grid is defined by some combination of these three vectors.

The frequency, Ω , is given as a vector $\Omega = [\omega_x, \omega_y]$, where ω_x and ω_y are the x and y components of the frequency. This vector has a direction, the direction of sampling, and length, which is a measure of frequency. The longer the vector, the higher the sampling frequency.

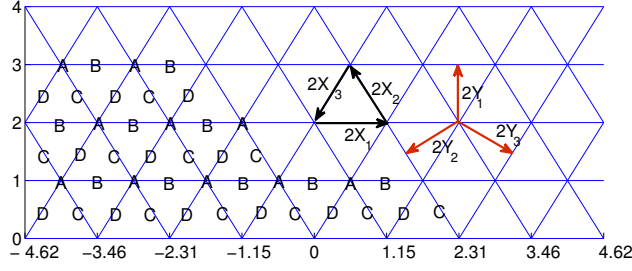


Figure 2: Parameter space of a triangle grid and the labelling used in Section 2. The mesh before refinement is shown in blue. The mesh after refinement is not shown. X_1 , X_2 and X_3 are shifts in the newly refined mesh. The grid directions are $X_1 = \left[\frac{1}{\sqrt{3}}, 0 \right]$, $X_2 = \left[-\frac{1}{2\sqrt{3}}, \frac{1}{2} \right]$ and $X_3 = \left[\frac{-1}{2\sqrt{3}}, \frac{1}{2} \right]$.

Let the input surface be $A_J = \cos(\pi\Omega \cdot 2J) + i \sin(\pi\Omega \cdot 2J) = e^{i\pi\Omega \cdot 2J} = T^{\Omega \cdot 2J}$, where $T = e^{i\pi}$. The samples are taken at $2J$, where $J = mX_1 + nX_2$, $m, n \in \mathbb{Z}$.

2.2. Artifacts after refinement

We assume the validity of the partitioning of the subdivision process into first a refinement stage followed by a series of convolutions with smoothing matrices as discussed by Sabin et al. (2005).

For simplicity, let A , B , C and D , as in Figure 2, be the magnitudes at vertices in the triangular mesh after refinement. So, the mesh after refinement has the entries

$$\begin{aligned} S_{2J} &= A T^{\Omega \cdot 2J} \\ S_{2J+X_1} &= B T^{\Omega \cdot (2J+X_1)} \\ S_{2J+X_2} &= C T^{\Omega \cdot (2J+X_2)} \\ S_{2J+X_3} &= D T^{\Omega \cdot (2J+X_2)} \end{aligned}$$

That is, each of the four types of vertex is a constant multiplied by the value of the surface that was sampled. The result of a refinement on a triangular mesh is to quadruple the original mesh points and insert zero values at all new positions B , C and D , so that $A = 4$ and $B = C = D = 0$ after refinement. This is equivalent to the quadrilateral case, discussed by Augsdörfer et al. (2009).

We partition the refined configuration into a component with only the original signal frequency and three artifact components. The artifacts cause displacements in magnitude of the original mesh points in the three directions along the grid lines. This implies that the artifacts introduce variations perpendicular to the grid lines. Therefore, the surface, S_P , where $P = 2J$, and which is made up of one signal and three artifact components, is given by

$$\begin{aligned} S_P &= T^{\Omega \cdot P} \\ &+ T^{\Omega \cdot P} \left(T^{Y_1 \cdot P} + T^{-Y_1 \cdot P} \right) / 2 \\ &+ T^{\Omega \cdot P} \left(T^{Y_2 \cdot P} + T^{-Y_2 \cdot P} \right) / 2 \\ &+ T^{\Omega \cdot P} \left(T^{Y_3 \cdot P} + T^{-Y_3 \cdot P} \right) / 2, \end{aligned}$$

where

$$Y_1 = \frac{1}{2}(X_2 - X_3), \quad Y_2 = \frac{1}{2}(X_3 - X_1), \quad \text{and} \quad Y_3 = \frac{1}{2}(X_1 - X_2)$$

are directions perpendicular to the grid lines, as shown in Figure 2.

Let a be the magnitude of the signal component and b , c and d be the magnitudes of the artifact components in the directions Y_1 , Y_2 and Y_3 respectively. Then the surface, S_P , after refinement is given by

$$\begin{aligned} S_P = & \quad a T^{\Omega.P} \\ & + b T^{\Omega.P} (T^{Y_1.P} + T^{-Y_1.P}) / 2 \\ & + c T^{\Omega.P} (T^{Y_2.P} + T^{-Y_2.P}) / 2 \\ & + d T^{\Omega.P} (T^{Y_3.P} + T^{-Y_3.P}) / 2, \end{aligned}$$

The relationships between the vertex values of the refined mesh and the signal and artifact magnitudes are

$$\begin{aligned} A &= (a + b + c + d) \\ B &= (a + b - c - d) \\ C &= (a - b + c - d) \\ D &= (a - b - c + d) \end{aligned}$$

In matrix notation this is

$$\begin{bmatrix} A \\ B \\ C \\ D \end{bmatrix} = \begin{bmatrix} 1 & 1 & 1 & 1 \\ 1 & 1 & -1 & -1 \\ 1 & -1 & 1 & -1 \\ 1 & -1 & -1 & 1 \end{bmatrix} \begin{bmatrix} a \\ b \\ c \\ d \end{bmatrix} = N \begin{bmatrix} a \\ b \\ c \\ d \end{bmatrix}. \quad (1)$$

The inverse of matrix N is simply $N^{-1} = N/4$. Hence, we have

$$\begin{bmatrix} a \\ b \\ c \\ d \end{bmatrix} = \frac{1}{4} \begin{bmatrix} 1 & 1 & 1 & 1 \\ 1 & 1 & -1 & -1 \\ 1 & -1 & 1 & -1 \\ 1 & -1 & -1 & 1 \end{bmatrix} \begin{bmatrix} A \\ B \\ C \\ D \end{bmatrix} = \frac{1}{4} N \begin{bmatrix} A \\ B \\ C \\ D \end{bmatrix} \quad (2)$$

Matrix N expresses therefore a two way relationship between the magnitudes at the refined vertices and the amount of signal and artifact components. After refinement each component has a unit magnitude, $a = b = c = d = 1$.

2.3. Artifacts after smoothing

A single smoothing stage in all three grid line directions of a triangular mesh is given by the mask:

$$\frac{1}{8} \begin{bmatrix} & 1 & & \\ 1 & & 2 & \\ & 1 & & 1 \end{bmatrix} \quad (3)$$

For example, one step of Loop subdivision can be implemented as a refinement stage followed by two of these smoothing stages.

Let A_s , B_s , C_s and D_s be the magnitudes at vertices in the triangular mesh after smoothing. The effect of applying the smoothing mask (3) to the refined data is thus

$$\begin{aligned} 8A_s &= 2A + 2B \cos(\pi\Omega.X_1) + 2C \cos(\pi\Omega.X_2) + 2D \cos(\pi\Omega.X_3) \\ 8B_s &= 2A \cos(\pi\Omega.X_1) + 2B + 2C \cos(\pi\Omega.X_3) + 2D \cos(\pi\Omega.X_2) \\ 8C_s &= 2A \cos(\pi\Omega.X_2) + 2B \cos(\pi\Omega.X_3) + 2C + 2D \cos(\pi\Omega.X_1) \\ 8D_s &= 2A \cos(\pi\Omega.X_3) + 2B \cos(\pi\Omega.X_2) + 2C \cos(\pi\Omega.X_1) + 2D \end{aligned}$$

Substituting c_1 , c_2 and c_3 for $\cos(\pi\Omega.X_1)$, $\cos(\pi\Omega.X_2)$ and $\cos(\pi\Omega.X_3)$ respectively, we can write the above in matrix notation as

$$\begin{bmatrix} A_s \\ B_s \\ C_s \\ D_s \end{bmatrix} = \frac{1}{4} \begin{bmatrix} 1 & c_1 & c_2 & c_3 \\ c_1 & 1 & c_3 & c_2 \\ c_2 & c_3 & 1 & c_1 \\ c_3 & c_2 & c_1 & 1 \end{bmatrix} \begin{bmatrix} A \\ B \\ C \\ D \end{bmatrix} = R \begin{bmatrix} A \\ B \\ C \\ D \end{bmatrix} \quad (4)$$

Equation (1) uses matrix N to encode the relationship between the vertex values A , B , C , D and the magnitudes of the signal and artifact components a , b , c , d . Equation (1) is also valid between smoothed data A_s , B_s , C_s , D_s and the magnitudes of the signal and artifact components a_s , b_s , c_s , d_s of the smoothed data. We thus have

$$\begin{bmatrix} a_s \\ b_s \\ c_s \\ d_s \end{bmatrix} = \frac{1}{4} NRN \begin{bmatrix} a \\ b \\ c \\ d \end{bmatrix} = R_N \begin{bmatrix} a \\ b \\ c \\ d \end{bmatrix} \quad (5)$$

where $R_N = NRN/4$:

$$R_N = \frac{1}{4} \begin{bmatrix} 1 + c_1 + c_2 + c_3 & 0 & 0 & 0 \\ 0 & 1 + c_1 - c_2 - c_3 & 0 & 0 \\ 0 & 0 & 1 - c_1 + c_2 - c_3 & 0 \\ 0 & 0 & 0 & 1 - c_1 - c_2 + c_3 \end{bmatrix}.$$

We can thus rewrite Equation (5) as

$$\begin{aligned} a_s &= a (1 + c_1 + c_2 + c_3)/4 \\ b_s &= b (1 + c_1 - c_2 - c_3)/4 \\ c_s &= c (1 - c_1 + c_2 - c_3)/4 \\ d_s &= d (1 - c_1 - c_2 + c_3)/4 \end{aligned}$$

We are now able to look at specific examples of sampling frequencies Ω .

If the sampling frequency is perpendicular to one of the grid lines, e.g. $\Omega = hY_1$, where $h \in \mathbb{R}$, we have $c_1 = \cos(\pi h Y_1.X_1) = 1$, $c_2 = \cos(\pi h Y_1.X_2) = 0$ and $c_3 = \cos(\pi h Y_1.X_3) = 0$. $(Y_1.X_2) = -(Y_1.X_3)$

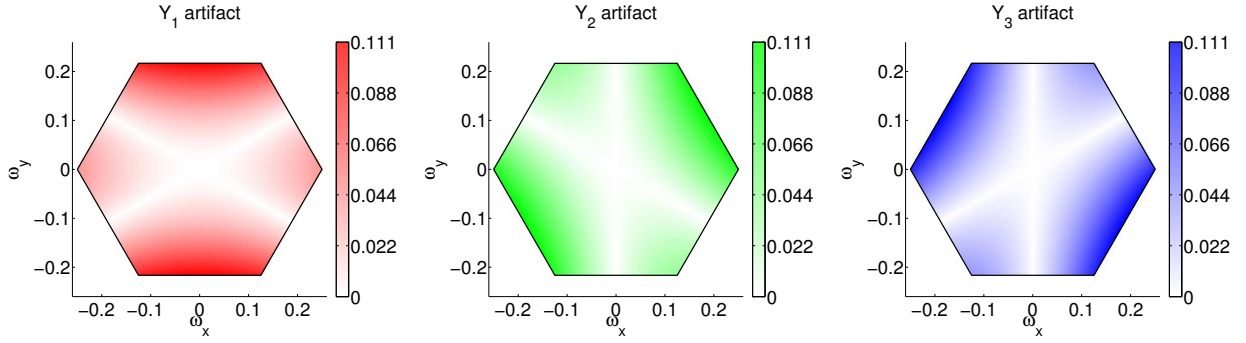


Figure 3: The three 2D plots of the hexagonal region of interest in the $\Omega = [\omega_x, \omega_y]$ parameter space of the three artifact components Y_1 , Y_2 and Y_3 respectively demonstrate the effect on the magnitude on the surface of a single smoothing stage after refinement in a triangular mesh on the three artifact components with respect to sampling frequency. By a symmetry argument it is clear that these are exactly rotated copies of one another.

and we therefore have $c_2 = c_3 = \cos(\pi\omega)$ where $\omega = hY_1 \cdot X_2$. For $\Omega = hY_1$ we thus have

$$\begin{aligned} a_s &= (2 + 2 \cos(\pi\omega))/4 &= \cos^2(\pi\omega/2) \\ b_s &= (2 - 2 \cos(\pi\omega))/4 &= \sin^2(\pi\omega/2) \\ c_s &= (1 - 1 + \cos(\pi\omega) - \cos(\pi\omega))/4 &= 0 \\ d_s &= (1 - 1 - \cos(\pi\omega) + \cos(\pi\omega))/4 &= 0 \end{aligned}$$

Therefore there are no artifacts in the Y_2 or Y_3 direction when the data is extruded along the X_1 direction, but there are artifacts in the Y_1 direction, perpendicular to the direction of the extrusion.

Similarly, when the data has an extrusion in direction X_2 or X_3 we do not get any artifacts in Y_1 or Y_3 direction, or Y_1 or Y_2 direction respectively. For sampling frequencies in directions other than perpendicular to the grid lines it is difficult to determine an analytic expression for the signal and artifact amplification. However, matrix R_N can be used to calculate signal and artifact magnitudes for any sampling frequency. Because

$$(NR^s N)/4 = (NRN/4)^s = R_N^s, \quad (6)$$

every additional smoothing term after refinement will simply increase the power on R_N and we can therefore determine the effect of additional smoothing stages on the magnitude of signal and artifact components by simply multiplying by R_N for each smoothing stage.

The effect of a single smoothing stage on each of the three artifact components can be determined independently as a function of sampling frequency $\Omega = [\omega_x, \omega_y]$ as shown in Figure 3.

The effect of smoothing on all artifact components present after refinement can be summarised by looking at the effect of smoothing on their sum, or at the mean artifact energy, given by $\sqrt{(b^2 + c^2 + d^2)/3}$, as in Figure 4. We can look at the effect of one, two or more smoothing stages.

Likewise, we look at the attenuation of the signal component after one smoothing stage as a function of sampling frequency. We also express the sum of artifacts as a percentage of the attenuated signal to demonstrate how much the initial signal has deteriorated in comparison to the artifact components, both shown in Figure 5.

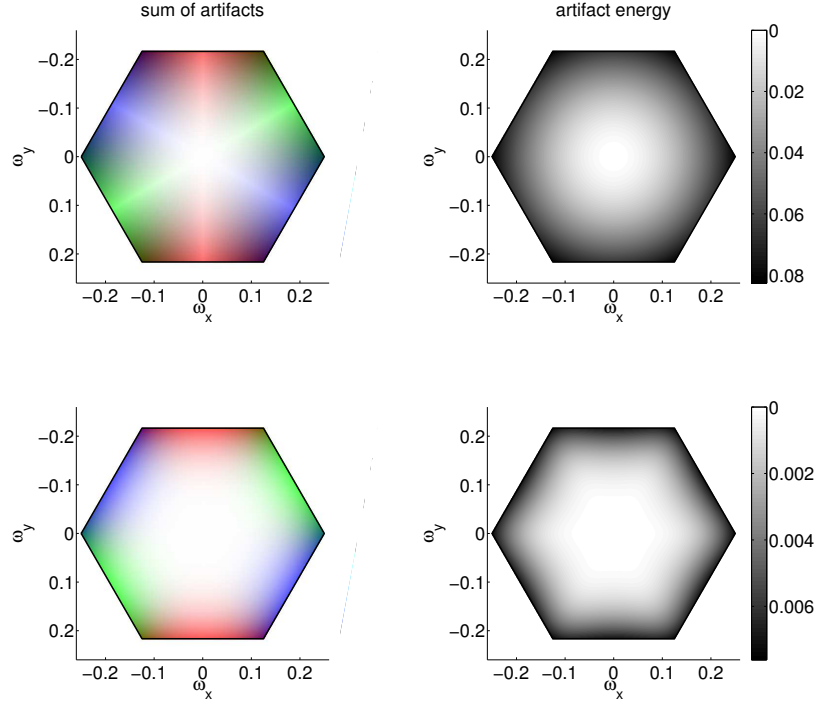


Figure 4: *Top: The sum of artifact components (left) and the mean energy of the artifact (right) are shown as a function of sampling frequency after one subdivision step including one smoothing stage in the three principal grid directions. Bottom: the same as above, but for a subdivision step with two smoothing stages. Note the difference in scale of a factor of 10.*

Both signal and artifact energy decrease with every additional smoothing stage in a single subdivision step. Also, with every additional subdivision step, the magnitude of the signal and artifact components introduced in the refinement stage of the first subdivision step decreases. For some engineering applications highly accurate surfaces are important and many subdivision steps are performed. So rather than looking at their magnitudes after only a single subdivision step we extend the analysis to determine the magnitudes in the limit surface, which are important to such CAD/CAE applications.

2.4. Artifacts in the limit

Matrix R_N enables us to compute the magnitudes of both signal and artifact term after one subdivision step. However, we are interested in the magnitudes of signal and artifact components in the limit surface, S_P , such that

$$\begin{aligned}
 S_P = & \alpha T^{\Omega,P} \\
 & + \beta T^{\Omega,P} (T^{Y_1,P} + T^{-Y_1,P}) / 2 \\
 & + \gamma T^{\Omega,P} (T^{Y_2,P} + T^{-Y_2,P}) / 2 \\
 & + \delta T^{\Omega,P} (T^{Y_3,P} + T^{-Y_3,P}) / 2
 \end{aligned} \tag{7}$$

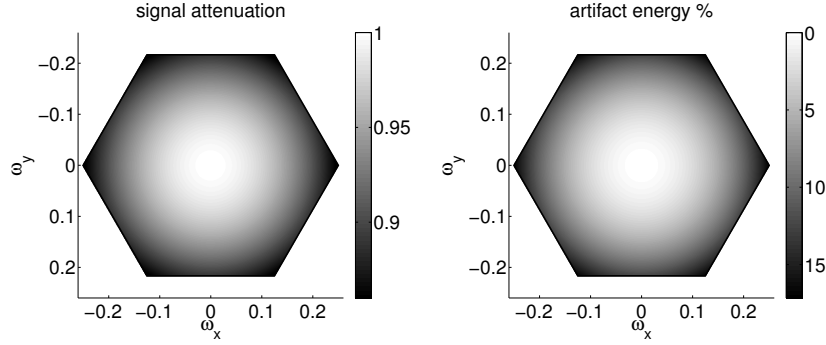


Figure 5: The signal attenuation (left) and the energy of the artifact as a percentage of signal (right) are shown after one subdivision step with one smoothing stage as a function of sampling frequency.

where α is the magnitude of the signal component in the limit and β , γ and δ are the magnitudes in the limit of the artifact components in the three directions Y_1 , Y_2 and Y_3 respectively.

To compute the magnitudes of signal and artifact term in the limit we consider the effect of the limit stencil on the data after one subdivision step. The limit stencil is derived from the row eigenvector corresponding to the dominant eigenvalue of the scheme (Halstead et al., 1993). We show an example in Section 3. By rewriting the limit stencil as a matrix similar to matrix R in Equation 5 we can derive the magnitudes of signal and artifact components in the limit. Let L be the limit matrix. Then we have

$$\begin{bmatrix} A_L \\ B_L \\ C_L \\ D_L \end{bmatrix} = L \begin{bmatrix} A_s \\ B_s \\ C_s \\ D_s \end{bmatrix} = LN \begin{bmatrix} a_s \\ b_s \\ c_s \\ d_s \end{bmatrix} = LNR_N^s \begin{bmatrix} a \\ b \\ c \\ d \end{bmatrix} \quad (8)$$

Where s is the number of smoothing stages of a particular scheme. Equation (1) holds for the limit data also. We thus have

$$\begin{bmatrix} \alpha \\ \beta \\ \gamma \\ \delta \end{bmatrix} = \frac{1}{4}NLNR_N^s \begin{bmatrix} a \\ b \\ c \\ d \end{bmatrix} = LNR_N^s \begin{bmatrix} a \\ b \\ c \\ d \end{bmatrix} \quad (9)$$

where $L_N = NLN/4$.

Because the limit stencils will be different for each subdivision scheme, we discuss the implementation in detail in the next section.

3. Examples

We present results for three triangular subdivision schemes: the Loop scheme (Loop, 1987), the Butterfly scheme (Dyn et al., 1990), and an interpolating scheme with two smoothing stages.

α	$\frac{(3 + c_1 + c_2 + c_3)(1 + c_1 + c_2 + c_3)^2}{96}$
β	$\frac{(3 + c_1 - c_2 - c_3)(1 + c_1 - c_2 - c_3)^2}{96}$
γ	$\frac{(3 - c_1 + c_2 - c_3)(1 - c_1 + c_2 - c_3)^2}{96}$
δ	$\frac{(3 - c_1 - c_2 + c_3)(1 - c_1 - c_2 + c_3)^2}{96}$

Table 1: The signal and artifact magnitudes in the limit surface when using the original Loop subdivision scheme, where α is the signal magnitude and β, γ and δ are the magnitudes of artifacts in the Y_1, Y_2 and Y_3 direction respectively. The expressions c_1, c_2 and c_3 stand for $\cos(\pi\Omega.X_1), \cos(\pi\Omega.X_2)$ and $\cos(\pi\Omega.X_3)$ respectively.

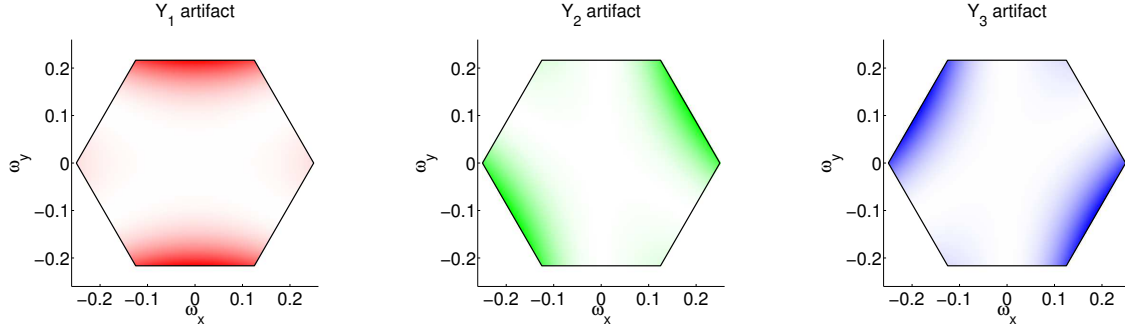


Figure 6: The three artifact components in the limit surface when using the original Loop scheme.

3.1. The Loop scheme

The mask of the Loop scheme (Loop, 1987) is

$$\frac{1}{16} \begin{bmatrix} & 1 & 2 & 1 & & \\ & 2 & 6 & 6 & 2 & \\ 1 & 6 & 10 & 6 & 6 & 1 \\ & 2 & 6 & 6 & 2 & \\ & 1 & 2 & 1 & & \end{bmatrix} \quad (10)$$

It is equivalent to the convolution of two smoothing masks (3). We therefore multiply the refined data by R_N^2 to determine the magnitudes of signal and artifacts after one subdivision step (e.g, see the bottom row of Figure 4).

To determine the magnitudes in the limit we derive a limit matrix, L , from the limit stencil of the scheme, which is determined from the dominant row eigenvector:

$$\begin{bmatrix} & 1 & 1 & \\ 1 & 6 & 1 & \\ & 1 & 1 & \end{bmatrix} / 12 \quad (11)$$

The effect of applying the limit stencil (11) to the data after one Loop subdivision step can then be described as

$$\begin{aligned} 12A_L &= 6A_s + 2B_s \cos(\pi\Omega.X_1) + 2C_s \cos(\pi\Omega.X_2) + 2D_s \cos(\pi\Omega.X_3) \\ 12B_L &= 2A_s \cos(\pi\Omega.X_1) + 6B_s + 2C_s \cos(\pi\Omega.X_3) + 2D_s \cos(\pi\Omega.X_2) \\ 12C_L &= 2A_s \cos(\pi\Omega.X_2) + 2B_s \cos(\pi\Omega.X_3) + 6C_s + 2D_s \cos(\pi\Omega.X_1) \\ 12D_L &= 2A_s \cos(\pi\Omega.X_3) + 2B_s \cos(\pi\Omega.X_2) + 2C_s \cos(\pi\Omega.X_1) + 6D_s \end{aligned}$$

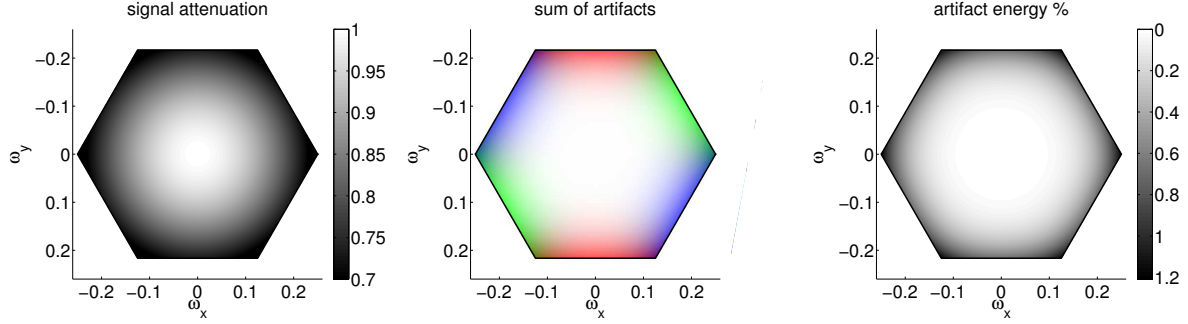


Figure 7: Magnitudes in the limit surface when applying the Loop scheme are shown as a function of sampling frequency. Left: The signal attenuation. Centre: The three artifacts Y_1 (red), Y_2 (green) and Y_3 (blue). Right: The artifact energy as a percentage of the attenuated signal (right).

Substituting c_1 , c_2 and c_3 for $\cos(\pi\Omega.X_1)$, $\cos(\pi\Omega.X_2)$ and $\cos(\pi\Omega.X_3)$ respectively, the matrix notation is

$$\begin{bmatrix} A_L \\ B_L \\ C_L \\ D_L \end{bmatrix} = \frac{1}{6} \begin{bmatrix} 3 & c_1 & c_2 & c_3 \\ c_1 & 3 & c_3 & c_2 \\ c_2 & c_3 & 3 & c_1 \\ c_3 & c_2 & c_1 & 3 \end{bmatrix} \begin{bmatrix} A_s \\ B_s \\ C_s \\ D_s \end{bmatrix} = L \begin{bmatrix} A_s \\ B_s \\ C_s \\ D_s \end{bmatrix}. \quad (12)$$

The magnitudes of the signal and artifact components in the limit are given by

$$\begin{bmatrix} \alpha \\ \beta \\ \gamma \\ \delta \end{bmatrix} = \frac{1}{4} NLNR_N^2 \begin{bmatrix} a \\ b \\ c \\ d \end{bmatrix} = L_N R_N^2 \begin{bmatrix} a \\ b \\ c \\ d \end{bmatrix}. \quad (13)$$

and $L_N = NLN/4$ is

$$L_N = \frac{1}{6} \begin{bmatrix} 3 + c_1 + c_2 + c_3 & 0 & 0 & 0 \\ 0 & 3 + c_1 - c_2 - c_3 & 0 & 0 \\ 0 & 0 & 3 - c_1 + c_2 - c_3 & 0 \\ 0 & 0 & 0 & 3 - c_1 - c_2 + c_3 \end{bmatrix}.$$

The magnitudes of the signal and artifact components in the limit are summarised in Table 1. We can now evaluate signal and artifact amplitudes in the limit for any sampling frequency. Each artifact component is shown separately in Figure 6. Results for signal attenuation, the sum of artifact components and the total artifact energy as a percentage of remaining signal are shown in Figure 7.

3.2. The Butterfly scheme

This is an interpolating scheme with a kernel from which no further smoothing stages can be extracted. The kernel can be dealt with in the same way we handle the smoothing stages.

The mask of the Butterfly scheme (Dyn et al., 1990) is

α	$\parallel \frac{(1 + 2(c_1 + c_2 + c_3) - (c_{12} + c_{13} + c_{23}))(1 + c_1 + c_2 + c_3)}{16}$
β	$\parallel \frac{(1 + 2(c_1 - c_2 - c_3) - (-c_{12} - c_{13} + c_{23}))(1 + c_1 - c_2 - c_3)}{16}$
γ	$\parallel \frac{(1 + 2(-c_1 + c_2 - c_3) - (-c_{12} + c_{13} - c_{23}))(1 - c_1 + c_2 - c_3)}{16}$
δ	$\parallel \frac{(1 + 2(-c_1 - c_2 + c_3) - (c_{12} - c_{13} - c_{23}))(1 - c_1 - c_2 + c_3)}{16}$

Table 2: The signal and artifact magnitudes in the limit surface when using the butterfly subdivision scheme, where α is the signal magnitude and β , γ and δ are the magnitudes of artifacts in the Y_1 , Y_2 and Y_3 direction respectively. The expressions c_1 , c_2 and c_3 stand for $\cos(\pi\Omega.X_1)$, $\cos(\pi\Omega.X_2)$ and $\cos(\pi\Omega.X_3)$ respectively, while c_{12} , c_{23} and c_{13} stand for $\cos(\pi\Omega.(X_1 - X_2))$, $\cos(\pi\Omega.(X_2 - X_3))$ and $\cos(\pi\Omega.(X_1 - X_3))$.

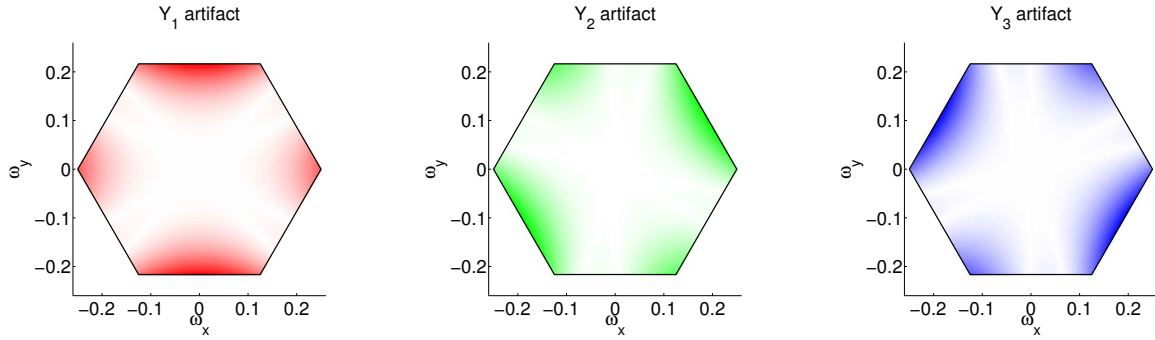


Figure 8: The three artifact components in the limit surface when using the butterfly scheme.

$$\frac{1}{16} \begin{bmatrix} & & & -1 & -1 & & & \\ & -1 & 0 & 2 & 0 & -1 & & \\ -1 & 2 & 8 & 8 & 2 & -1 & & \\ & 0 & 8 & 16 & 8 & 0 & & \\ -1 & 2 & 8 & 8 & 2 & -1 & & \\ & -1 & 0 & 2 & 0 & -1 & & \\ & & & -1 & -1 & & & \end{bmatrix}.$$

This is the smoothing mask (3) convolved with the kernel mask:

$$\frac{1}{8} \begin{bmatrix} & & & -1 & & & & \\ & -1 & 2 & 2 & -1 & & & \\ & 2 & 2 & 2 & & & & \\ -1 & 2 & 2 & -1 & & & & \\ & & & -1 & & & & \end{bmatrix}. \quad (14)$$

Let A_{sk} , B_{sk} , C_{sk} and D_{sk} be the magnitudes at vertices in the triangular mesh after the kernel has been applied. The vertex magnitudes are laid out as shown in Figure 2. The effect of applying the kernel mask (14) to the refined and smoothed data is

$$8A_{sk} = 2A_s + B_s(4 \cos(\pi\Omega.X_1) - 2 \cos(\pi\Omega.(X_2 - X_3)))$$

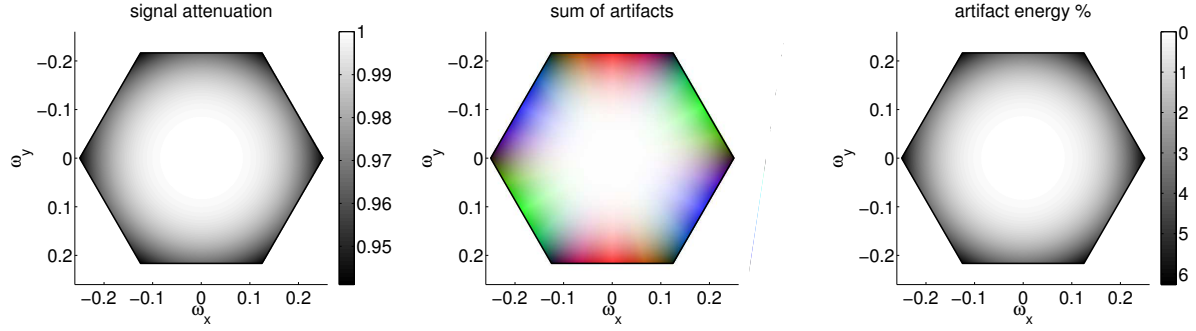


Figure 9: Magnitudes in the limit for the butterfly scheme as a function of sampling frequency. Left: The signal attenuation. Centre: The three artifacts Y_1 (red), Y_2 (green) and Y_3 (blue). Right: The artifact energy as a percentage of the attenuated signal.

$$\begin{aligned}
& +C_s(4 \cos(\pi\Omega.X_2) - 2 \cos(\pi\Omega.(X_1 - X_3))) \\
& +D_s(4 \cos(\pi\Omega.X_3) - 2 \cos(\pi\Omega.(X_1 - X_2))) \\
8B_{sk} = & A_s(4 \cos(\pi\Omega.X_1) - 2 \cos(\pi\Omega.(X_2 - X_3))) \\
& +2B_s \\
& +C_s(4 \cos(\pi\Omega.X_3) - 2 \cos(\pi\Omega.(X_1 - X_2))) \\
& +D_s(4 \cos(\pi\Omega.X_2) - 2 \cos(\pi\Omega.(X_1 - X_3))) \\
8C_{sk} = & A_s(4 \cos(\pi\Omega.X_2) - 2 \cos(\pi\Omega.(X_1 - X_3))) \\
& +B_s(4 \cos(\pi\Omega.X_3) - 2 \cos(\pi\Omega.(X_1 - X_2))) \\
& +2C_s \\
& +D_s(4 \cos(\pi\Omega.X_1) - 2 \cos(\pi\Omega.(X_2 - X_3))) \\
8D_{sk} = & A_s(4 \cos(\pi\Omega.X_3) - 2 \cos(\pi\Omega.(X_1 - X_2))) \\
& +B_s(4 \cos(\pi\Omega.X_2) - 2 \cos(\pi\Omega.(X_1 - X_3))) \\
& +C_s(4 \cos(\pi\Omega.X_1) - 2 \cos(\pi\Omega.(X_2 - X_3))) \\
& +2D_s
\end{aligned}$$

Substituting c_1 , c_2 and c_3 for $\cos(\pi\Omega.X_1)$, $\cos(\pi\Omega.X_2)$ and $\cos(\pi\Omega.X_3)$ respectively, and c_{12} , c_{23} and c_{13} for $\cos(\pi\Omega.(X_1 - X_2))$, $\cos(\pi\Omega.(X_2 - X_3))$ and $\cos(\pi\Omega.(X_1 - X_3))$ we write the above in matrix notation as

$$\begin{bmatrix} A_{sk} \\ B_{sk} \\ C_{sk} \\ D_{sk} \end{bmatrix} = \frac{1}{4} \begin{bmatrix} 1 & 2c_1 - c_{23} & 2c_2 - c_{13} & 2c_3 - c_{12} \\ 2c_1 - c_{23} & 1 & 2c_3 - c_{12} & 2c_2 - c_{13} \\ 2c_2 - c_{13} & 2c_3 - c_{12} & 1 & 2c_1 - c_{23} \\ 2c_3 - c_{12} & 2c_2 - c_{13} & 2c_1 - c_{23} & 1 \end{bmatrix} \begin{bmatrix} A_s \\ B_s \\ C_s \\ D_s \end{bmatrix} = K \begin{bmatrix} A_s \\ B_s \\ C_s \\ D_s \end{bmatrix} \quad (15)$$

We therefore can determine the signal and artifact magnitude after one step of butterfly subdivision

as

$$\begin{bmatrix} a_{sk} \\ b_{sk} \\ c_{sk} \\ d_{sk} \end{bmatrix} = \frac{1}{4} NKNR_N \begin{bmatrix} a \\ b \\ c \\ d \end{bmatrix} = K_N R_N \begin{bmatrix} a \\ b \\ c \\ d \end{bmatrix} \quad (16)$$

where $K_N = NKN/4$.

This gives

$$\begin{aligned} a_{sk} &= (1 + 2c_1 - c_{23} + 2c_2 - c_{13} + 2c_3 - c_{12})/4 \times (1 + c_1 + c_2 + c_3)/4 \\ b_{sk} &= (1 + 2c_1 - c_{23} - 2c_2 + c_{13} - 2c_3 + c_{12})/4 \times (1 + c_1 - c_2 - c_3)/4 \\ c_{sk} &= (1 - 2c_1 + c_{23} + 2c_2 - c_{13} - 2c_3 + c_{12})/4 \times (1 - c_1 + c_2 - c_3)/4 \\ d_{sk} &= (1 - 2c_1 + c_{23} - 2c_2 + c_{13} + 2c_3 - c_{12})/4 \times (1 - c_1 - c_2 + c_3)/4 \end{aligned}$$

Because the scheme is interpolating the magnitudes determined in this way also apply to the limit surface. The results are summarised in Table 2. The magnitudes of three artifact components are shown individually in Figure 8. The signal magnitude, the sum of the three artifact components and the corresponding artifact energy as a percentage of remaining signal in the limit are shown in Figure 9.

3.3. An interpolating scheme with two smoothing stages

We now consider a novel scheme which, like the Loop scheme (Loop, 1987) discussed in Section 3.1, has two smoothing stages in each of the grid directions but, unlike the Loop scheme, interpolates original control points. We construct this by designing the kernel K to give interpolation while having a small a footprint as possible. The scheme has the following mask:

$$\frac{1}{64} \begin{bmatrix} & & -1 & -3 & -3 & -1 & & & \\ & & -3 & 0 & 6 & 0 & -3 & & \\ -1 & -3 & 6 & 33 & 33 & 6 & -3 & & \\ & -3 & 6 & 33 & 33 & 6 & -3 & -1 & \\ & & -3 & 0 & 6 & 0 & -3 & & \\ & & & -1 & -3 & -3 & -1 & & \end{bmatrix}. \quad (17)$$

This is equivalent to the convolution of two smoothing masks (3) and a kernel mask given by

$$K = \frac{1}{4} \begin{bmatrix} & -1 & -1 & \\ -1 & & 10 & -1 \\ & -1 & -1 & \end{bmatrix}. \quad (18)$$

The kernel is treated as before. Let A_{sk} , B_{sk} , C_{sk} and D_{sk} be the magnitudes at vertices in the triangular mesh after the kernel has been applied to the refined and smoothed data. The effect of

α	$\frac{(5 - c_1 - c_2 - c_3)(1 + c_1 + c_2 + c_3)^2/32}{(5 - c_1 + c_2 + c_3)(1 + c_1 - c_2 - c_3)^2/32}$
β	$\frac{(5 - c_1 + c_2 + c_3)(1 + c_1 - c_2 - c_3)^2/32}{(5 + c_1 - c_2 + c_3)(1 - c_1 + c_2 - c_3)^2/32}$
γ	$\frac{(5 + c_1 - c_2 + c_3)(1 - c_1 + c_2 - c_3)^2/32}{(5 + c_1 + c_2 - c_3)(1 - c_1 - c_2 + c_3)^2/32}$
δ	$\frac{(5 + c_1 + c_2 - c_3)(1 - c_1 - c_2 + c_3)^2/32}{(5 - c_1 - c_2 - c_3)(1 + c_1 + c_2 + c_3)^2/32}$

Table 3: The signal and artifact magnitudes in the limit surface when using the interpolating Loop subdivision scheme, where α is the signal magnitude and β, γ and δ are the magnitudes of artifacts in the Y_1, Y_2 and Y_3 direction respectively. The expressions c_1, c_2 and c_3 stand for $\cos(\pi\Omega.X_1), \cos(\pi\Omega.X_2)$ and $\cos(\pi\Omega.X_3)$ respectively.

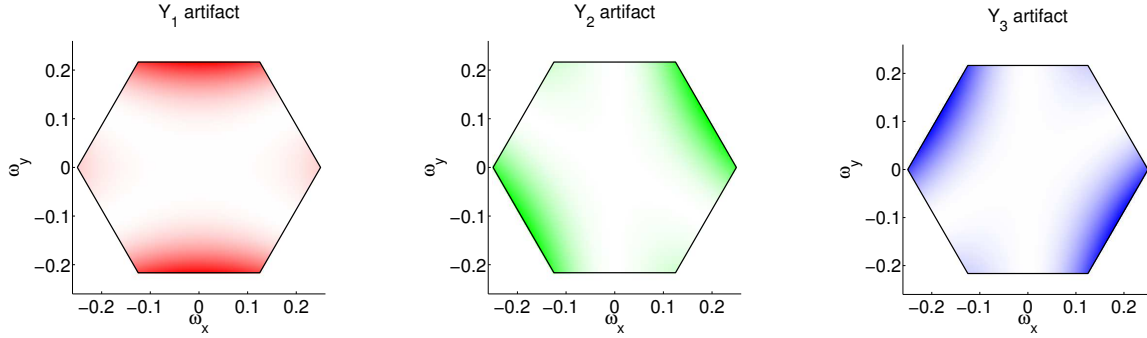


Figure 10: The three artifact components in the limit surface when using the interpolating Loop scheme.

applying the kernel can then be described as

$$\begin{aligned}
4A_{sk} &= 10A_s - 2B_s \cos(\pi\Omega.X_1) - 2C_s \cos(\pi\Omega.X_2) - 2D_s \cos(\pi\Omega.X_3) \\
4B_{sk} &= -2A_s \cos(\pi\Omega.X_1) + 10B_s - 2C_s \cos(\pi\Omega.X_3) - 2D_s \cos(\pi\Omega.X_2) \\
4C_{sk} &= -2A_s \cos(\pi\Omega.X_2) - 2B_s \cos(\pi\Omega.X_3) + 10C_s - 2D_s \cos(\pi\Omega.X_1) \\
4D_{sk} &= -2A_s \cos(\pi\Omega.X_3) - 2B_s \cos(\pi\Omega.X_2) - 2C_s \cos(\pi\Omega.X_1) + 10D_s
\end{aligned}$$

Substituting c_1, c_2 and c_3 for $\cos(\pi\Omega.X_1/2), \cos(\pi\Omega.X_2/2)$ and $\cos(\pi\Omega.X_3/2)$ respectively, the matrix notation is

$$\begin{bmatrix} A_{sk} \\ B_{sk} \\ C_{sk} \\ D_{sk} \end{bmatrix} = \frac{1}{4} \begin{bmatrix} 10 & -2c_1 & -2c_2 & -2c_3 \\ -2c_1 & 10 & -2c_3 & -2c_2 \\ -2c_2 & -2c_3 & 10 & -2c_1 \\ -2c_3 & -2c_2 & -2c_1 & 10 \end{bmatrix} \begin{bmatrix} A_s \\ B_s \\ C_s \\ D_s \end{bmatrix} = \frac{1}{4} K \begin{bmatrix} A_s \\ B_s \\ C_s \\ D_s \end{bmatrix}. \quad (19)$$

We therefore can determine the signal and artifact magnitude after one step of subdivision as

$$\begin{bmatrix} a_{sk} \\ b_{sk} \\ c_{sk} \\ d_{sk} \end{bmatrix} = \frac{1}{4} N K N R_N^2 \begin{bmatrix} a \\ b \\ c \\ d \end{bmatrix} = K_N R_N^2 \begin{bmatrix} a \\ b \\ c \\ d \end{bmatrix}, \quad (20)$$

where $K_N = NKN/4$. This can be rewritten as

$$\begin{aligned}
a_{sk} &= (10 - 2c_1 - 2c_2 - 2c_3)/4 \times (1 + c_1 + c_2 + c_3)^2/16 \\
b_{sk} &= (10 - 2c_1 + 2c_2 + 2c_3)/4 \times (1 + c_1 - c_2 - c_3)^2/16 \\
c_{sk} &= (10 + 2c_1 - 2c_2 + 2c_3)/4 \times (1 - c_1 + c_2 - c_3)^2/16 \\
d_{sk} &= (10 + 2c_1 + 2c_2 - 2c_3)/4 \times (1 - c_1 - c_2 + c_3)^2/16.
\end{aligned}$$

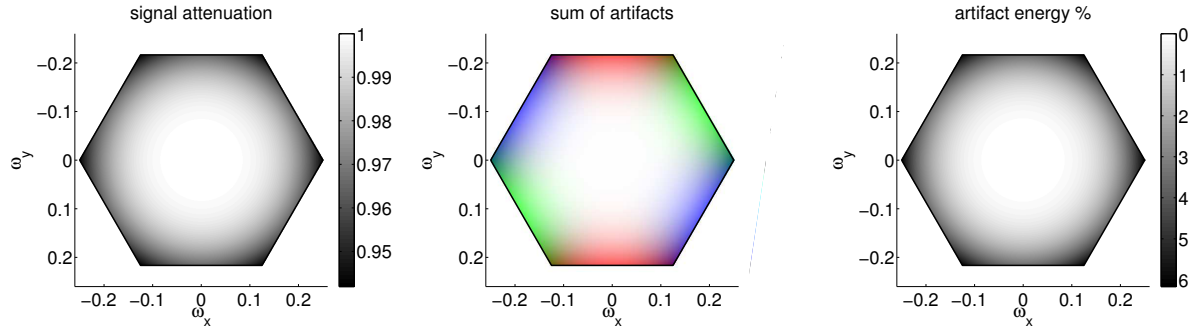


Figure 11: Magnitudes in the limit for the interpolating scheme with two smoothing stages shown as a function of sampling frequency. Left: The signal attenuation. Centre: The three artifacts Y_1 (red), Y_2 (green) and Y_3 (blue). Right: The artifact energy as a percentage of the attenuated signal.

Because the scheme is interpolating the magnitudes determined in this way also apply to the limit surface. The result is summarised in Table 3.

4. Summary and Discussion

We apply subdivision as a tool of analysis to determine the magnitude of signal and artifact components in box-spline and subdivision surfaces.

One subdivision step can be viewed as a multi-stage process involving a refinement stage followed by one or more smoothing stages. We can analyse the effect of each factor on the input data separately. We show that artifact components are inevitably introduced in the refinement stage. For a binary subdivision step the surface after refinement is made up of a signal component and three artifact components correspondent to the grid lines. The signal and the artifact components are then smoothed out in subsequent smoothing stages.

When handling schemes not based on box-splines we may encounter, alongside refinement and smoothing stages, a kernel from which no more smoothing stages can be extracted. The kernel can be analysed employing the same mechanism used to establish the effect of smoothing. By analysing the effect of the smoothing stages and the kernel on both the input signal and the artifact components introduced during refinement, we are able to make a statement about their magnitude after one subdivision step.

The magnitude of the signal and artifact component after one subdivision step will be further reduced with further subdivision steps. For high end engineering applications many subdivision steps are needed to achieve the required accuracy of subdivision limit surfaces. From the eigenstructure of the subdivision matrix we derive a limit stencil which is employed to derive artifact magnitudes on the limit surface of a particular scheme.

The previously presented framework for analysing artifacts present in the limit surfaces (Sabin et al., 2005; Augsdörfer et al., 2009) proved difficult to apply to surfaces based on triangular meshes. The work presented here shows a framework that is easily applied to triangular schemes. We derive generic expression in matrix form for the effects of refinement and smoothing is further extended to account for a kernel and determine the effect in the limit. We demonstrate the

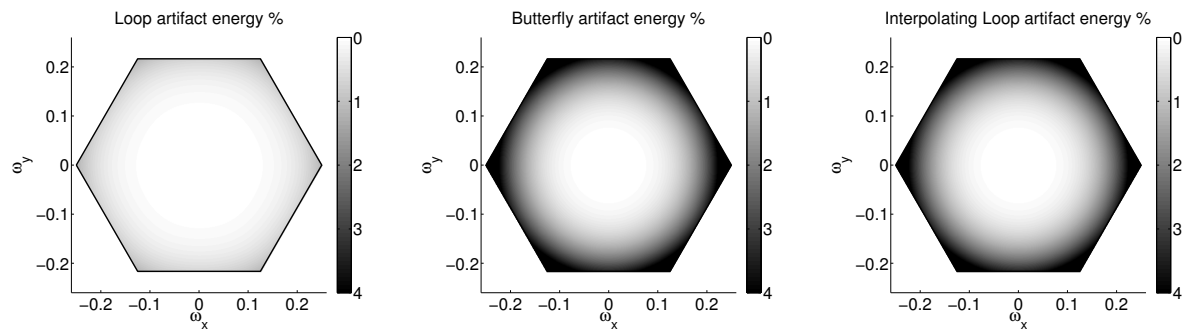


Figure 12: The artifact energy as a function of remaining signal for the three schemes analysed, all shown with the same scale: The Loop (left), the Butterfly (centre) and the interpolating Loop scheme (right).

framework by analysing box-spline and subdivision surfaces based on triangular meshes. Three schemes are analysed: Loop subdivision (Loop, 1987), Butterfly subdivision (Dyn et al., 1990) and a novel interpolating scheme with two smoothing stages.

As expected both interpolating subdivision schemes retain the initial signal information well. However, due to large artifacts introduced in the limit surfaces, these schemes will be made up of a higher percentage of artifact than the limit surface of the Loop subdivision scheme, see Figure 12.

The key observation is that Loop is far more tolerant to features sampled near the Nyquist limit than are the interpolating schemes. The practical outcome of this is that the interpolating schemes need a higher density of vertices in the initial sampling mesh to achieve the same quality of limit surface.

References

- Augsdörfer, U., Dodgson, N., Sabin, M., 2009. Artifact analysis on B-splines and quadrilateral subdivision surfaces. submitted to Computer Aided Geometric Design.
- Dyn, N., Levin, D., Gregory, J., 1990. A butterfly subdivision scheme for surface interpolation with tension control. *ACM Transactions on Graphics* 9 (2), 160–169.
- Halstead, M., Kass, M., DeRose, T., 1993. Efficient, fair interpolation using catmull-clark surfaces. In: *Computer Graphics Proceedings, Annual Conference Series, 1993. ACM SIGGRAPH*. pp. 35–44.
- Loop, C., 1987. Smooth subdivision surfaces based on triangles. Master’s thesis, Department of Mathematics, University of Utah.
- Sabin, M., Augsdorfer, U., Dodgson, N., 2005. Artifacts in box-spline surfaces. In: *Mathematics of Surfaces XI*. pp. 350–363.
- Sabin, M., Barthe, L., 2003. Artifacts in recursive subdivision surfaces. In: *Curve and Surface fitting: Saint-Malo 2002*. Nashboro Press, Brentwood, TN, pp. 353–362.